Nanograting-Enhanced Optical Fibers for Visible and Infrared Light Collection at Large Input Angles

Ning Wang [1,2,*], Matthias Zeisberger [3], Uwe Hübner [3] and Markus A. Schmidt [3,4,5,*]

1 Institute of Advanced Technology, Westlake Institute for Advanced Study, 18 Shilongshan Road, Hangzhou 310024, China
2 School of Engineering, Westlake University, 18 Shilongshan Road, Hangzhou 310024, China
3 Leibniz Institute of Photonic Technology, Albert-Einstein-Str. 9, 07745 Jena, Germany; matthias.zeisberger@leibniz-ipht.de (M.Z.); uwe.huebner@leibniz-ipht.de (U.H.)
4 Faculty of Physics, Abbe School of Photonics, Max-Wien-Platz 1, 07743 Jena, Germany
5 Otto Schott Institute of Materials Research, Fraunhoferstr. 6, 07743 Jena, Germany
* Correspondence: wangning@westlake.edu.cn (N.W.); markus.schmidt@leibniz-ipht.de (M.A.S.)

Abstract: The efficient incoupling of light into particular fibers at large angles is essential for a multitude of applications; however, this is difficult to achieve with commonly used fibers due to low numerical aperture. Here, we demonstrate that commonly used optical fibers functionalized with arrays of metallic nanodots show substantially improved large-angle light-collection performances at multiple wavelengths. In particular, we show that at visible wavelengths, higher diffraction orders contribute significantly to the light-coupling efficiency, independent of the incident polarization, with a dominant excitation of the fundamental mode. The experimental observation is confirmed by an analytical model, which directly suggests further improvement in incoupling efficiency through the use of powerful nanostructures such as metasurface or dielectric gratings. Therefore, our concept paves the way for high-performance fiber-based optical devices and is particularly relevant within the context of endoscopic-type applications in life science and light collection within quantum technology.

Keywords: fiber optics; plasmonic gratings; nanodot; light collection

1. Introduction

Over the past half century, optical fiber has revolutionized modern telecommunication technology and industry from various perspectives [1–3]. Up to today, optical fiber research still represents a major scientific field within the optics community with applications ranging from highly efficient bio-sensor devices [4–7] to broadband light sources [8–10]. However, suffering from a small numerical aperture (e.g., the NA of single-mode fiber 28 (SMF-28) is only 0.14 at λ = 1550 nm), the light collection efficiency of commonly used step-index fibers is insufficient for many applications and cannot satisfy the demands of emerging applications such as wide-field endoscopes [11] or quantum photon probes [12]. To address this challenge, we have recently introduced a universal approach for improving the light-incoupling ability of optical fibers through integrating plasmonic nanodot arrays [13] and dielectric concentric rings [14] on end faces of SMF-28. Through exploiting different diffraction orders, this leads to significant improvements in coupling efficiency, especially at very large angles at infrared wavelengths. In the present work, we extend the spectral range of this concept and experimentally demonstrate a significant improvement of light-coupling efficiencies across a wide incident angle interval (30° < θ < 85°) at selected visible and infrared wavelengths. We specifically choose 550 nm as one of the excitation wavelengths to investigate the coupling concept at such a short wavelength, whereas the measurements at 1650 nm serve as a reference. Note that, theoretically, at

any individual wavelength within the spectral range (i.e., from 550 nm to 1650 nm), the coupling efficiencies can be improved by our approach.

　　The structure targeted here is schematically illustrated in Figure 1a. Here, an SMF-28 fiber tip functionalized by an array of hexagonally arranged gold nanodots is excited by either a p- or a s- polarized beam (indicated by a green arrow) under an incident angle of θ (wavelength λ). The grating deflects a certain amount of transmitted power to a defined diffraction order (for example, the -1st order is illustrated in Figure 1a by a dark red arrow). The diffracted light couples to the fiber modes, leading to an enhancement of the light-coupling efficiencies at angles that otherwise show little coupling efficiency in case of a fiber with an unstructured interface. The incoupling efficiency η is defined here as $\eta(\theta) = P_{out} / P_{in}$, where P_{out} and P_{in} are the fiber output and input powers, respectively (see labels 'P_{out}' and 'P_{in}' in Figure 1a). Note that, in the following, we use the normalized incoupling efficiency defined as $\eta_{norm}(\theta) = \eta(\theta)/\eta(\theta = 0°)$ to clearly highlight the increases in value enabled by the nanostructures.
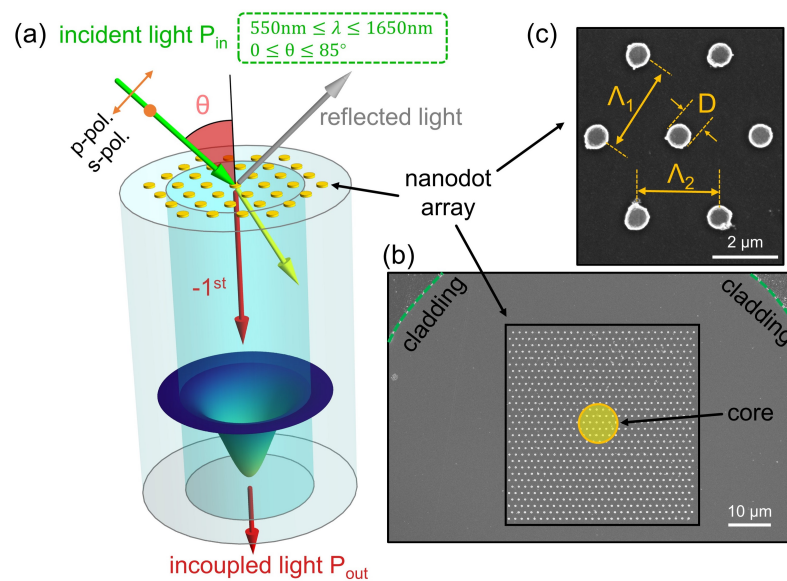

Figure 1. A schematic (**a**) illustrating the concept of the nanoarray-assisted fiber-based light collection at incoupling angles of θ. (**b**,**c**): The scanning electron microscopy (SEM) images of gold nanodot array (D: 480 nm, Λ_1: 1.9 μm, Λ_2: 1.7 μm) located at the core section of an SMF-28. In (**b**), the orange shadow denotes the fiber mode area.

2. Theoretical Toy Model Analysis

　　For understanding the light-coupling process from a semi-quantitative perspective, we utilize a strongly simplified one-dimensional scalar model [15] to describe the coupling efficiency/incident angle dependence $\eta = \eta(\theta)$ at a fixed wavelength. The model is based on the electric field integral between the fundamental fiber mode (HE_{11}-mode) and the exciting wave just below the nanostructure that is partially generated by the nanodot grating (the model is depicted in Figure 2a). In the case of SMF-28, the HE_{11} mode can be approximated by a Gaussian profile ($E \approx exp(\frac{x^2}{w^2})$) due to the weak guidance approximation, and the excitation field is assumed to be a plane wave (wavelength λ, wavenumber $k_0 = 2\pi/\lambda$). Note that, as mentioned above for theoretical analysis, we normalize the coupling efficiency to its value at perpendicular incidence $\eta_{norm}(\theta) = \eta(\theta)/\eta(\theta = 0°)$. As the first step, we defined the coupling strength $C_b(\theta)$ parameter to characterize the coupling into a fiber with no nanostructure:

$$C_b(\theta) \sim \cos\theta \left| \int_{-\infty}^{\infty} e^{\frac{-x^2}{w^2}} e^{ik_x x} dx \right|^2 \tag{1}$$

where k_x is the projection of wavenumber k_0 along the x-axis ($k_x = k_0 \sin \theta$). The normalized coupling efficiency of the bare fiber $\eta_b(\theta)$ is then defined as $\eta_b(\theta) = C_b(\theta)/C_b(0)$.

By placing a plasmonic nanodot array (interdot distance (pitch) Λ) on the fiber facet, the corresponding nth diffraction order modifies the projection of the wave vector on the x-axis, and thus replaces k_x by $(k_x + nG)$ (lattice vector $G = \frac{2\pi}{\Lambda}$). Therefore, the coupling strength $C_g(\theta)$ is changed to:

$$C_g(\theta) \sim \cos \theta \left| \int_{-\infty}^{\infty} e^{\frac{-x^2}{w^2}} \sum_n a_n e^{i(k_x + nG)x} dx \right|^2 \qquad (2)$$

Here, the coefficients a_n represent the relative amplitudes of the diffracted waves. The summation covers all possible diffraction orders in the medium below the grating including the non-diffracted wave ($n = 0$). As a result of this modification, the nanograting-enhanced coupling efficiency follows the equation $\eta_g(\theta) = C_g(\theta)/C_g(0)$. Note that, for the shortest wavelength used in this work ($\lambda = 550$ nm), both $-$1st and $-$2nd orders (i.e., $n = -1$ or $n = -2$) contribute to efficiency enhancement, while for $\lambda = 1650$ nm only the $-$1st order (i.e., $n = -1$) is relevant. In addition to the two mentioned wavelengths, the toy model suggests that nanograting enhanced light-incoupling concept should principally work for any wavelength within the demonstrated spectral range.
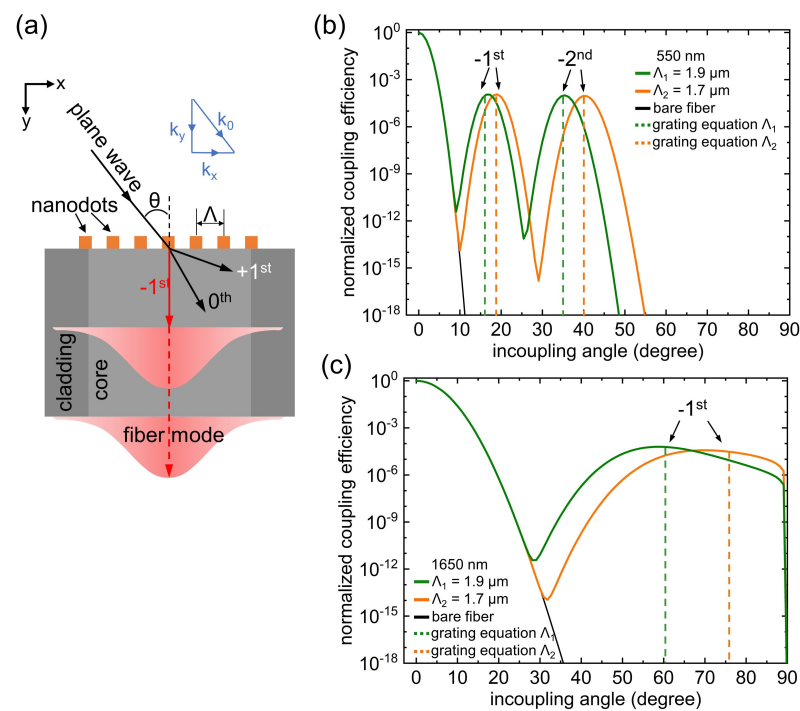

Figure 2. A theoretical model (**a**) of fiber light-coupling efficiencies for calculations at wavelengths of 550 nm (**b**) and 1650 nm (**c**), respectively. The dashed vertical lines in (**b**,**c**) correspond to additional enhancement position calculated by the grating equation.

The theoretical efficiencies $\eta_{norm}(\theta)$ at $\lambda = 550$ nm and $\lambda = 1650$ nm are plotted in Figure 2b,c, respectively. For the coefficients of the diffracted waves, we have used $a_n = 0.1$, which are estimated by the amount of scattered power which is in the order of the filling factor of the grating taking into account the distribution of the power across four diffracted waves. Note that the toy model represents a coarse approximation of the experimental circumstances and should only be qualitatively compared to experimental results. In each diagram, the black curve represents bare fibers, which all fail to operate beyond angles of 20° ($\eta < 10^{-6}$). In addition to the maximum value at normal incidence ($\theta = 0°$), nanostructure-enhanced fibers exhibit substantially improved incoupling efficien-

cies particularly at the angles labeled as '−1st' and '−2nd' (refer as local maxima), in which the overall amplitude is close to the order of 10^{-4}. It is notable that different pitches (green line: Λ_1 = 1.9 μm, orange line: Λ_2 = 1.7 μm) could modify the line shape of η and thus lead to an additional degree of freedom to vary the local maxima. For instance, in the case of the short wavelength (λ = 550 nm), the maximum of the −2nd peak for Λ = 1.9 μm (green line in Figure 2b) is located at around 35°, while for the Λ = 1.7 μm the counterpart (orange line) of this maximum approaches 40° (see the vertical dashed lines in Figure 2b).

As shown in ref. [13], the angles of maximal incoupling are related to the lattice constants of the grating and can be approximated by a diffraction order equation, which is given by $\theta = arc\sin(\frac{-n\lambda}{\Lambda})$ [16] and in particular includes the diffraction order n. For the short wavelength (λ = 550 nm), two maxima from two diffraction orders (−1st (n = −1) and −2nd (n = −2)) induce a substantial improvement in incoupling efficiency, while only the −1st order contributes to the case of the long wavelength (λ = 1650 nm), as already shown in ref. [13]. This effect is clearly visible from the diffraction order equation: the shorter wavelength contributes two values of incidence angle θ (λ = 550 nm, Λ_1 = 1.9 μm, $\theta_{-1st} \approx 17°$ and $\theta_{-2nd} \approx 35°$), whereas only one value of θ exists for the identical incidence scenario for the long wavelength (λ = 1650 nm, Λ_1 = 1.9 μm, $\theta_{-1st} \approx 60°$).

Here, we would like to point out that the SMF-28 exhibits higher-order modes at λ = 550 nm, which would demand including the respective modes in the theoretical model. However, our simple analytical model (Figure 2) shows good agreement with experimental data hereafter despite the mode differences. This is partially because the power fraction of fundamental mode dominates, and the higher modes have no major influence on the line shape of the light-incoupling efficiency. Therefore, we believe this simplified model is valuable in revealing the overall characteristics of the light-incoupling process for the configuration investigated here and the errors caused by the multimodeness are sufficiently small.

3. Implementation and Characterization Setup

The array of hexagonal nanodots (lattice constant Λ_1 = 1.9 μm and Λ_2 = 1.7 μm, scanning electron microscopy (SEM) images presented in Figure 1b,c) are fabricated on a cleaved end face of an SMF-28 using of modified electron beam lithography (more manufacturing details can be found in ref. [13]). The nanodots have diameters and thicknesses of D = 480 nm and t = 40 nm, resulting in a plasmonic resonance at around λ = 1440 nm with the full width at half maximum (FWHM) of 200 nm (a measured transmission spectrum is provided in ref. [13]).

The coupling efficiencies have been measured at various incidence configurations using a laser source (NKT Photonics SuperK Compact) together with several polarizers (Thorlabs), focusing lenses (Thorlabs) as well as power detectors (Thorlabs). More details to the typical setup are provided in ref. [13]. Note that, due to the detection limit of the powermeter used, several points could not be detected for $\theta > 50°$.

4. Experimental Results

The measured data at λ = 550 nm and λ = 1650 nm are presented in Figure 3a–d, overall showing a strong impact of the nanodot array on incoupling efficiency. In general, for both wavelengths the coupling efficiencies of nanostructure-enhanced fiber have been improved to the maximum of about 10^{-4} at large incidence angles (i.e., from 20° to 85°), while the distributions of local maxima strongly vary depending on wavelength and pitch. In addition to the value maximum at normal incidence (θ = 0°), two less-distinguished local maxima emerge at around θ = 20° and θ = 50° for λ = 550 nm (more obvious for the green dots), while only one local maximum (around 50°) was observed for λ = 1650 nm. This agrees with the theoretical model where both −1st and −2nd diffraction orders contribute at shorter wavelengths, while only the −1st order is relevant when the pitch value approximates the operation wavelength. Once again, the local maximum position of all four figures can be predicted by the simple formula $\theta = arc\sin(\frac{-n\lambda}{\Lambda})$, which are indicated

as color-coded dashed lines in Figure 3. The local maxima position mismatch between experiments and model predictions can be attributed to beam excitation differences (Gaussian beam in experiment while the plane wave excitation in toy model) and fluctuations of fabricated nanodot grating. Note that the line shape of the incoupling efficiency does not depend strongly on the incidence polarization. Additionally, we have carried out an additional efficiency measurement at 650 nm, resembling the data at 550 nm. Specifically, the overall efficiencies are improved at angles of 30° and 55°, indicating the involvement of both first and second diffraction orders.
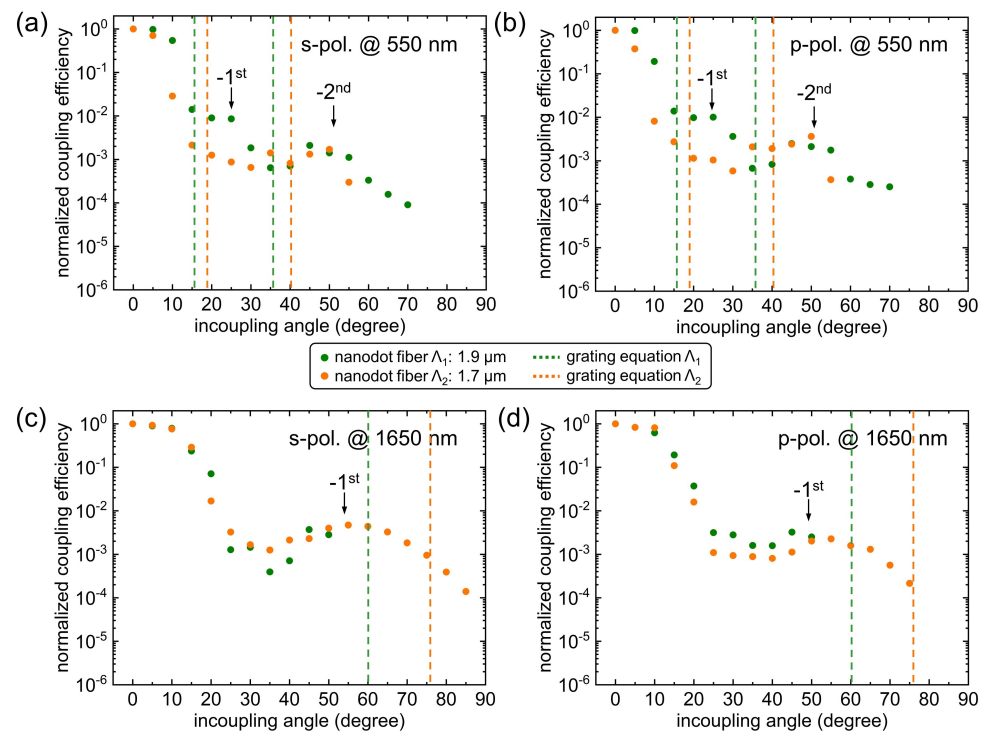

Figure 3. Experimental coupling efficiencies at wavelengths of 550 nm (**a**,**b**) and 1650 nm (**c**,**d**) under various incidence occasions (wavelength, angle, polarization, pitch condition, etc.). The vertical dashed lines situated at different incoupling angles have been obtained from the grating equation (i.e., $\theta = arc\sin(\frac{-n\lambda}{\Lambda})$) and the two colors refer to varied pitch configurations (green: Λ_1 = 1.9 μm, orange: Λ_2= 1.7 μm).

5. Conclusions

Even though optical fibers have been used to great success in a multitude of areas, collecting light under large angles within different spectral regimes remains a key challenge with commonly used fibers due to low numerical aperture. To meet this requirement, we demonstrate in this work that optical fibers functionalized with arrays of metallic nanodots located on the core of the fiber substantially improve light-collection performance at multiple wavelengths, extending the spectral domain of operation towards the visible. We experimentally demonstrate a nanostructure-mediated enhancement of the light-coupling efficiencies at large incident angles (from 30° to 85°) at two selected wavelengths (550 nm to 1650 nm), while nanostructure implementation relies on modified electron beam lithography. The overall improvement lies within the order of 10^{-4}, which can be improved in the future by optimization of disk diameter and thickness, while the the additional maximum in the angle spectrum at visible wavelengths is related to an additional diffraction orders.

Our concept represents a generic approach to increase light-coupling efficiencies and can easily be further improved by using high-performance nanostructures such as metasurfaces [17,18]. Note that commonly used multimode fibers have typical numerical apertures of at NA = 0.5 [19], yielding maximum incoupling angles of θ = 30°. This is substantially smaller than what can be achieved with our concept, emphasizing the

importance of nanostructure-mediated incoupling. Therefore, we strongly believe that the concept of light incoupling through nanostructures will have great impacts in various fields of research and applications including bioanalytics (e.g., collection of Raman signals [20]), life science (e.g., in vivo endoscopy [21]) or quantum technology (e.g., collection of light from single emitters [22]). We would like to emphasize that particular applications that require incoupling at large angles would benefit from the presented concept (e.g., in vivo imaging).

Author Contributions: M.A.S. conceived the idea. N.W. conducted the measurements and data analysis. M.Z. and N.W. performed the theory calculations. U.H. fabricated the sample. M.A.S. supervised the research. The manuscript was written by N.W., M.Z. and M.A.S. through contributions of all authors. All authors have read and agreed to the published version of the manuscript.

Institutional Review Board Statement: Not applicable.

Informed Consent Statement: Not applicable.

Data Availability Statement: Data is contained within the article.

Conflicts of Interest: The authors declare no conflict of interest.

References

1. Ghatak, A.A.; Ghatak, A.; Thyagarajan, K.; Thyagarajan, K. *An Introduction to Fiber Optics*; Cambridge University Press: Cambridge, UK, 1998.
2. Miller, S. *Optical Fiber Telecommunications*; Elsevier: Amsterdam, The Netherlands, 2012.
3. Alexander Schmidt, M.; Argyros, A.; Sorin, F. Hybrid optical fibers-an innovative platform for in-fiber photonic devices. *Adv. Opt. Mater.* **2016**, *4*, 13–36. [CrossRef]
4. Leung, A.; Shankar, P.M.; Mutharasan, R. A review of fiber-optic biosensors. *Sens. Actuators B Chem.* **2007**, *125*, 688–703. [CrossRef]
5. Doherty, B.; Csáki, A.; Thiele, M.; Zeisberger, M.; Schwuchow, A.; Kobelke, J.; Fritzsche, W.; Schmidt, M.A. Nanoparticle functionalised small-core suspended-core fibre–a novel platform for efficient sensing. *Biomed. Opt. Express* **2017**, *8*, 790–799. [CrossRef] [PubMed]
6. Wang, N.; Zeisberger, M.; Hübner, U.; Schmidt, M.A. Nanotrimer enhanced optical fiber tips implemented by electron beam lithography. *Opt. Mater. Express* **2018**, *8*, 2246–2255. [CrossRef]
7. Hong, Y.; Zhao, D.; Wang, J.; Lu, J.; Yao, G.; Liu, D.; Luo, H.; Li, Q.; Qiu, M. Solvent-Free Nanofabrication Based on Ice-Assisted Electron-Beam Lithography. *Nano Lett.* **2020**, *20*, 8841–8846. [CrossRef] [PubMed]
8. Chemnitz, M.; Gebhardt, M.; Gaida, C.; Stutzki, F.; Kobelke, J.; Limpert, J.; Tünnermann, A.; Schmidt, M.A. Hybrid soliton dynamics in liquid-core fibres. *Nat. Commun.* **2017**, *8*, 42. [CrossRef]
9. Sollapur, R.; Kartashov, D.; Zürch, M.; Hoffmann, A.; Grigorova, T.; Sauer, G.; Hartung, A.; Schwuchow, A.; Bierlich, J.; Kobelke, J.; et al. Resonance-enhanced multi-octave supercontinuum generation in antiresonant hollow-core fibers. *Light. Sci. Appl.* **2017**, *6*, e17124. [CrossRef]
10. Klas, R.; Kirsche, A.; Gebhardt, M.; Buldt, J.; Stark, H.; Hädrich, S.; Rothhardt, J.; Limpert, J. Ultra-short-pulse high-average-power Megahertz-repetition-rate coherent extreme-ultraviolet light source. *PhotoniX* **2021**, *2*, 1–8. [CrossRef]
11. Choi, Y.; Yoon, C.; Kim, M.; Yang, T.D.; Fang-Yen, C.; Dasari, R.R.; Lee, K.J.; Choi, W. Scanner-free and wide-field endoscopic imaging by using a single multimode optical fiber. *Phys. Rev. Lett.* **2012**, *109*, 203901. [CrossRef] [PubMed]
12. Bovino, F.A.; Varisco, P.; Colla, A.M.; Castagnoli, G.; Di Giuseppe, G.; Sergienko, A.V. Effective fiber-coupling of entangled photons for quantum communication. *Opt. Commun.* **2003**, *227*, 343–348. [CrossRef]
13. Wang, N.; Zeisberger, M.; Hübner, U.; Schmidt, M.A. Boosting light collection efficiency of optical fibers using metallic nanostructures. *ACS Photonics* **2019**, *6*, 691–698. [CrossRef]
14. Yermakov, O.; Schneidewind, H.; Hübner, U.; Wieduwilt, T.; Zeisberger, M.; Bogdanov, A.; Kivshar, Y.; Schmidt, M.A. Nanostructure-empowered efficient coupling of light into optical fibers at extraordinarily large angles. *ACS Photonics* **2020**, *7*, 2834–2841. [CrossRef]
15. Snyder, A.W.; Love, J. *Optical Waveguide Theory*; Springer Science & Business Media: Berlin/Heidelberg, Germany, 2012.
16. Saleh, B.E.; Teich, M.C. *Fundamentals of Photonics*; John Wiley & Sons: Hoboken, NJ, USA, 2019.
17. Khorasaninejad, M.; Capasso, F. Metalenses: Versatile multifunctional photonic components. *Science* **2017**, *358*. [CrossRef] [PubMed]
18. Zou, X.; Zheng, G.; Yuan, Q.; Zang, W.; Chen, R.; Li, T.; Li, L.; Wang, S.; Wang, Z.; Zhu, S. Imaging based on metalenses. *PhotoniX* **2020**, *1*, 1–24. [CrossRef]

19. Thorlabs. 0.50 NA Step-Index Multimode Fibers. Available online: https://www.thorlabs.com/newgrouppage9.cfm?objectgroup_id=362 (accessed on 16 June 2021).
20. Cordero, E.; Latka, I.; Matthäus, C.; Schie, I.W.; Popp, J. In-vivo Raman spectroscopy: From basics to applications. *J. Biomed. Opt.* **2018**, *23*, 071210. [CrossRef] [PubMed]
21. Pahlevaninezhad, H.; Khorasaninejad, M.; Huang, Y.W.; Shi, Z.; Hariri, L.P.; Adams, D.C.; Ding, V.; Zhu, A.; Qiu, C.W.; Capasso, F.; et al. Nano-optic endoscope for high-resolution optical coherence tomography in vivo. *Nat. Photonics* **2018**, *12*, 540–547. [CrossRef] [PubMed]
22. Li, X.; Scully, R.A.; Shayan, K.; Luo, Y.; Strauf, S. Near-unity light collection efficiency from quantum emitters in boron nitride by coupling to metallo-dielectric antennas. *ACS Nano* **2019**, *13*, 6992–6997. [CrossRef] [PubMed]